Continuous electrochemical water splitting from natural water sources via forward osmosis

Samuel S. Veroneau[a] and Daniel G. Nocera[a,1]

[a]Department of Chemistry and Chemical Biology, Harvard University, Cambridge, MA 02138

Contributed by Daniel G. Nocera, December 30, 2020 (sent for review December 3, 2020; reviewed by Curtis P. Berlinguette, Daniel V. Esposito, and Marc Koper)

Electrochemical water splitting stores energy as equivalents of hydrogen and oxygen and presents a potential route to the scalable storage of renewable energy. Widespread implementation of such energy storage, however, will be facilitated by abundant and accessible sources of water. We describe herein a means of utilizing impure water sources (e.g., saltwater) for electrochemical water splitting by leveraging forward osmosis. A concentration gradient induces the flow of water from an impure water source into a more concentrated designed electrolyte. This concentration gradient may subsequently be maintained by water splitting, where rates of water influx (i.e., forward osmosis) and effective outflux (i.e., water splitting) are balanced. This approach of coupling forward osmosis to water splitting allows for the use of impure and natural sources without pretreatment and with minimal losses in energy efficiency.

forward osmosis | water splitting | seawater | hydrogen | solar

Despite the abundance of renewable energy sources (e.g., solar and wind), their storage at scale remains limited (1–3). Compared to conventional means of energy storage, fuels produced by water splitting, either directly in the form of H_2 and O_2 (4) or indirectly in the form of liquid fuels via artificial photosynthesis (5–8), offer greater energy density and scalability. The keystone water-splitting process may be driven electrochemically via the hydrogen evolution (HER) and oxygen evolution half-reactions (OER) (1, 9, 10). Whereas the focus of most endeavors has been on the development of catalysts that operate in purified water sources, 96.5% of global water reserves exist as brackish water and seawater (11). As such, the development of water splitting at scale will be facilitated by the development of approaches that can directly use natural water sources (12–15). Although natural water sources are abundant, they are corrosive to most earth-abundant catalysts at neutral pHs and unavoidably contain impurities including dissolved salts, organic molecules, and particulates. Some of these challenges have been overcome with the development of self-healing water-splitting catalysts (16–18) and in the case of seawater, with the design of catalyst matrices that are able to reject interfering anions such as chloride and bromide (19–21). A more conventional approach involves prepurification of water sources prior to use by reverse osmosis and related approaches (21–25).

We now report an approach that leverages electrochemical water splitting with passive forward osmosis to allow for sustained water splitting from impure water sources with minimal losses in efficiency. Water splitting drives an effective outflux of H_2O by its conversion into H_2 and O_2 gases that in turn generates a concentration gradient, which is balanced with an influx of H_2O provided by forward osmosis. By setting rates of influx and outflux equal, H_2O is continually extracted from an impure water source via forward osmosis and purified H_2O is provided for water splitting. A 0.6 M NaCl solution is used as a surrogate for seawater as sodium (Na^+) and chloride (Cl^-) are the predominant ions responsible for the salinity of seawater. We show that the forward osmosis–water splitting (FOWS) permits the simultaneous and equivalent influx and effective outflux of H_2O over prolonged operation while allowing for HER and OER to proceed at unit faradaic efficiency with the rejection of the Cl^- ion, thus allowing for a simple way to accomplish selective hydrogen and oxygen generation from saltwater. Our results show that the FOWS design allows for the use of conventional and stable electrodes for water splitting from impure sources that operate at high current densities.

Results

Fig. 1 illustrates the general design principles for the FOWS cell, which comprises a single electrochemical compartment segregated from an impure water source with a semipermeable membrane. The FOWS cell chamber was an inverted 15-mL centrifuge tube in which a Pt mesh anode and cathode and an Ag/AgCl reference electrode resided. The FOWS cell was charged with 10 mL of 0.8 M NaP_i inner electrolyte buffered at pH 7 and was separated from 0.6 M NaCl outer solution using a cellulose acetate (26, 27) semipermeable membrane (Fig. 1*A*). A 0.2 M concentration gradient was chosen to accommodate electrochemical water splitting at the applied current of 250 mA (*vide infra*). For these experiments, a volume of 1.5 L was chosen for the outer solution so that the salt concentration was approximately constant over the course of the experiment, thus providing for a relatively constant osmotic pressure.

Electrochemical water splitting performed at 250 mA resulted in a stable operating potential of ∼2.80 V vs. standard hydrogen electrode (SHE) over a 48-h period (Fig. 2*A*). The observed ±0.185-V variability of the operating potential was due to the formation of

Significance

The growing need for the widespread adoption of renewable energy necessitates scalable energy storage. A potential route to meeting this challenge is electrochemical water splitting driven by renewable energy that will require, at scale, abundant and accessible sources of water. Recognizing that 96.5% of global water reserves exist as brackish water and seawater, water splitting approaches utilizing these sources and other impure water sources are warranted. The approach described here couples water splitting with forward osmosis to enable saltwater to be utilized directly without pretreatment or purification while circumventing the challenges posed by impurities and parasitic energy-wasting side reactions.

Author contributions: S.S.V. and D.G.N. designed research; S.S.V. performed research; S.S.V. contributed new reagents/analytic tools; S.S.V. and D.G.N. analyzed data; and S.S.V. and D.G.N. wrote the paper.

Reviewers: C.P.B., University of British Columbia; D.V.E., Columbia University; and M.K., Leiden University.

The authors declare no competing interest.

[1]To whom correspondence may be addressed. Email: dnocera@fas.harvard.edu.

This article contains supporting information online at https://www.pnas.org/lookup/suppl/doi:10.1073/pnas.2024855118/-/DCSupplemental.

Published February 22, 2021.

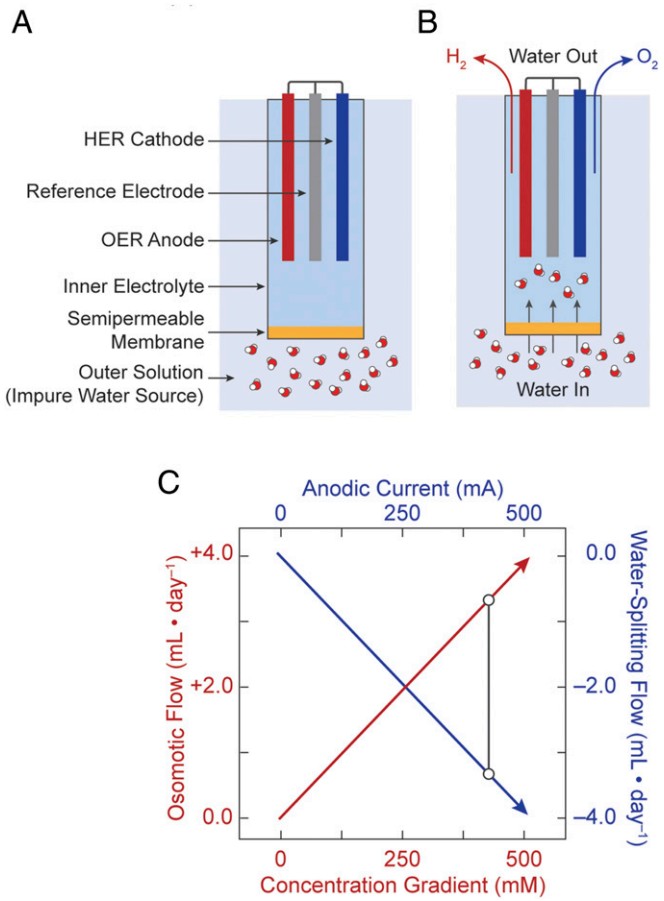

Fig. 1. Schematic overview of FOWS cell. (*A*) Basic components of FOWS cell for operation in impure water sources. (*B*) Processes underlying FOWS cell operation with the concurrent water influx via forward osmosis and effective water outflux via electrochemical water splitting. (*C*) Plot of rates of water influx (red) and outflux (blue) as calculated from Eqs. **1** and **2**, respectively, where the rates are equivalent when the anodic current and concentration gradient are properly balanced. These rates are equivalent at any point along any vertical line (e.g., black bar).

transient gas bubbles on the reference electrode. Gas chromatography (GC) analysis of the FOWS cell headspace was performed hourly throughout the 48-h period. As the faradaic efficiency for water splitting is 100% (Fig. 2 *C* and *D*), sustained operation of the FOWS cell at 250 mA corresponds to an effective outflux of ~2.02 mL H_2O per day, which would result in a depletion of ~40% of the internal volume without a compensating influx of H_2O. Notwithstanding, the internal volume of FOWS cell increased by ~0.25 mL within the first day of operation after which the system attained steady state and the solution volume remained constant with continued operation.

To assess whether phosphate (P_i) leached from the FOWS cell, a Malachite green phosphate assay (28) was performed on the outer solution at timepoints of 0, 24, and 48 h of operation. As summarized in Fig. 3*A*, less than 3 molar % of the total P_i concentration is found to leach through the semipermeable membrane into the outer solution after 48 h. This corresponds to a rate of leaching for P_i of ~4.7 μmol·h^{-1}, as compared to water splitting occurring at 2.3 mmol·h^{-1}. To quantify the passage of Cl^- into the inner electrolyte solution of the FOWS cell, a Lucigenin fluorescent probe was used (29). Similar to the results for P_i, 0.4 mmol of Cl^- was found to accumulate in inner electrolyte solution (Fig. 3*B*) after 24 h, occupying ~4% of the inner electrolyte based on total electrolyte concentration of 0.8 M, after which the concentration of Cl^- remained constant. The observed steady-state Cl^- concentration suggested Cl^- consumption at the anode. The expected products of such oxidation at neutral pH and room temperature are HClO and ClO^- based on the Pourbaix diagram (30). These products were quantified using a *N*,*N*-diethyl-p-phenylenediamine (DPD) assay (31). Less than 3 μmol of HClO/ClO^- were found to accumulate in the FOWS cell after 48 h (Fig. 3*C*). The Cl^- oxidation accounts for <0.001% loss in faradaic efficiency and hence is not reflected in the GC-measured water-splitting faradaic efficiency (Fig. 2 *C* and *D*). Additionally, the measured HER/OER faradaic efficiencies suggest minimal gas cross-over or other parasitic reductive and oxidative processes that compete with electrochemical water splitting. A summary of the operational metrics of the FOWS cell is compiled in Table 1.

Discussion

The influx of H_2O (mL·s^{-1}) into an FOWS cell via forward osmosis is proportional to the provided concentration gradient between the inner electrolyte and external water source, as described with the follow equation:

$$q_{influx} = \mathcal{I}\mathrm{RT}\frac{K_w S}{d}\Delta C, \quad [1]$$

where K_w is the membrane permeability coefficient for water (mL·atm^{-1}·s^{-1}·cm^{-1}), S is the membrane surface area (cm^2), d is the membrane thickness (cm), $\mathcal{I}$ is the van't Hoff factor, R is the ideal gas constant (L·atm·K^{-1}·mol^{-1}), T is the temperature (K), and ΔC is the concentration gradient (M). Eq. **1** assumes hydraulic forces to be negligible. The effective outflux of H_2O from an FOWS cell via electrochemical water splitting (units: mL·s^{-1}) is proportional to the current passed through the system,

$$q_{outflux} = \frac{i\mathrm{V_m}}{2\mathrm{F}}, \quad [2]$$

where i here is the current (A), V_m is the molar volume of H_2O (mL·mol^{-1}), and F is Faraday's constant (C·mol^{-1}). At a steady state, where the volume within the FOWS cell is constant, the rates of H_2O influx and outflux are equivalent,

$$\left|q_{outflux}\right| = \left|q_{influx}\right|. \quad [3]$$

Equating Eqs. **1** and **2**,

$$i\frac{V_m}{2F} = (\mathcal{I}RT)\frac{K_w S}{d}\Delta C, \quad [4]$$

and rearranging Eq. **4** furnishes the steady-state condition for the current passed to the concentration gradient,

$$i/\Delta C = (\mathcal{I}RT)\left(\frac{K_w S}{d}\right)\left(\frac{2F}{V_m}\right). \quad [5]$$

By determining Eq. **5**, the steady-state ratio of current to concentration gradient may be approximated. The product of the van't Hoff index $\mathcal{I}$ and membrane permeability coefficient for water K_w may be estimated from Eq. **1** by measuring the rate of influx, q_{influx}, through the cellulose acetate membrane at a known concentration gradient ΔC in the absence of water splitting. For an FOWS cell charged with 0.8 M NaP_i and placed in a 0.6 M NaCl solution the change in inner volume of the cell was monitored over a 4-h period revealing a rate of influx of

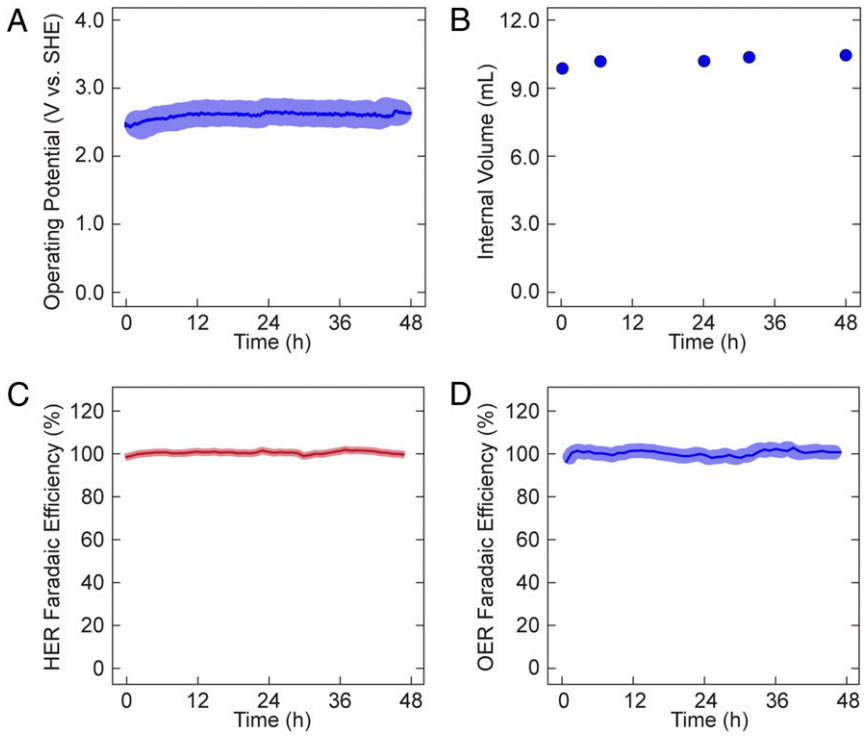

Fig. 2. Assessment of electrochemical water splitting in FOWS cell. (*A*) Chronopotentiometry at 250 mA with a 0.8 M NaP_i inner electrolyte solution and 0.6 M NaCl outer electrolyte solution. Average operation potential (blue line) with observed SD of measurements (light-blue halo). (*B*) Observed water level within the FOWS cell over period of operation. (*C*) Average faradaic efficiency for HER (red line) with observed SD of measurements (light-red halo) over 48-h period of operation. (*D*) Average faradaic efficiency for OER (blue line) with observed SD of measurements (light-blue halo) over 48-h period of operation.

$q_{influx} = 0.08\ \text{mL}\cdot\text{h}^{-1}$ (or $1.92\ \text{mL}\cdot\text{day}^{-1}$) for the defined $\Delta C = 0.2$ M. Solving for Eq. **5** gives

$$i/\Delta C = 1.05\ \text{A}\cdot\text{M}^{-1}. \quad \textbf{[6]}$$

For the cellulose acetate membrane with dimensions of $S = 1\ \text{cm}^2$ and $d = 1$ mm, Eq. **6** defines that a steady-state concentration gradient 0.95 M is maintained by an electrochemical water-splitting current of 1 A. Thus, to maintain the 0.2 M concentration gradient of the FOWS cell described herein, an applied current of 210 mA is needed for water splitting. A slightly higher current of 250 mA was chosen to allow a steady state to be attained gradually with the internal volume slightly decreasing. The slight initial increase (2.5%) in the inner electrolyte volume prior to attaining steady-state conditions indicates slightly underestimated values from our measurement of passive forward osmosis. Excepting this minor discrepancy, the result of steady-state operation of the FOWS cell at 250 mA validates Eq. **6** in practice and establishes that the concurrent processes of forward osmosis and electrochemical water splitting may maintain a designed concentration gradient. To corroborate this, a separate FOWS cell was charged with 0.7 NaP_i and placed in a 0.6 M NaCl solution, whereupon a current of 125 mA was applied, again resulting in steady-state operation for several days.

The FOWS cell purifies a natural water source by passive forward osmosis. This is demonstrated by the comparison of water splitting in a 0.6 M saltwater electrolyte vs. in the FOWS cell. Within the error of measurement, 100% faradaic efficiencies are observed for water splitting in the FOWS cell as compared to 50 and 20% faradaic efficiencies for HER and OER, respectively, in the 0.6 M saltwater electrolyte (*SI Appendix*, Fig. S5). Such lower faradaic efficiencies are consistent with Cl^- oxidation with the caveat that a membrane is not used to separate the anode and cathode in the FOWS cell. Hence the decrease in faradaic efficiency is also due to significant cross-over of Cl^- oxidation products (32). The marginal leaching of P_i from the FOWS cell and influx of Cl^- into the FOWS cell (Fig. 3 *A* and *B*) establishes that the overall FOWS approach offers a novel means of performing water splitting from natural water sources.

The passage of Cl^- and P_i is a direct consequence of the selectivity offered by the semipermeable cellulose acetate membrane, which was chosen owing to its availability and ubiquity. Improvements of this FOWS approach will rely largely upon membranes that can accommodate high flowrates with enhanced selectivity. For instance, the energy efficiency of the system depends on the water-splitting potential. The use of Pt electrodes in neutral water is suboptimal for efficient water splitting. Water splitting in base or acid solutions will greatly improve the energy efficiency but ion-selective membranes that are stable to concentrated base or acid will be required. Additionally, the design of FOWS cells with well-separated anode and cathode compartments, as well as designing internal compartments including anion-exchange membranes, could benefit the practicality and effectiveness of this approach.

Conclusion

By coupling water splitting to forward osmosis, a concentration gradient may be maintained to provide continual flow of H_2O for electrochemical water splitting from impure water sources that may include brackish water and seawater. In this regard, the FOWS cell design adds (*SI Appendix*) a new approach to the widespread implementation of scalable renewable energy storage by allowing for the use of impure water splitting for the generation of H_2 and O_2 while avoiding separate purification and desalination processes.

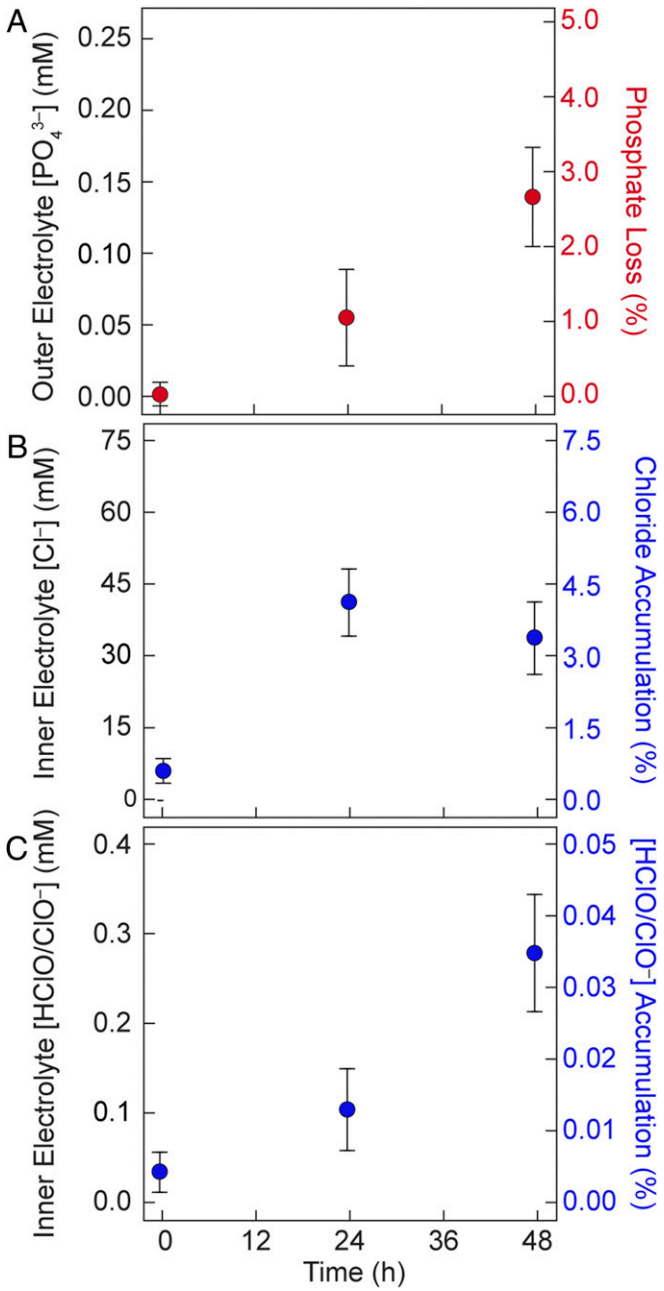

Fig. 3. Assessment of ion flow of the FOWS cell. (*A*) Quantification of phosphate (P_i) ions in outer solution over 48 h of operation. Axes describe total concentration of P_i in outer solution (*Left*) and percentage of P_i that leached out of the FOWS cell (*Right*). (*B*) Quantification of Cl^- ions in inner electrolyte solution over 48 h of operation. Axes describe total concentration of Cl^- (*Left*) and as percentage of Cl^- (*Right*) within the FOWS cell. (*C*) Quantification of HClO/ClO^- ions in inner electrolyte solution over 48 h of operation. Axes describe total concentration (*Left*) and as percentage (*Right*) of HClO/ClO^- within the FOWS cell (*Right*).

Materials and Methods

Materials. NaH_2PO_4 was used as received from Fischer. NaOH (<0.001% Ni, Fe, and other heavy metals) was used as received from EMD Millipore. All electrolyte solutions were prepared with type I water (EMD Millipore, 18.2 MΩ cm resistivity). Pt wire (0.5-mm diameter, 99.95% metal basis) and Pt gauze (52 mesh, 99.9% metal basis) were obtained from Alfa Aesar and soaked overnight in 50% HNO_3 in type I water prior to use. A leak-free Ag/AgCl reference electrode (2 mm, length 65 mm, 1 mm gold-plated pin, < 30 kΩ) was obtained from Warner Instruments. A 305 mm × 305 mm FTS H_2O flat sheet membrane (1121820, cellulose triacetate, forward osmosis) was obtained from Sterlitech and rinsed three times with type I water prior to use.

FOWS Cell Construction and Electrochemical Measurements. The conical end of a Falcon 15-mL polypropylene conical tube was cut at the 2-mL gradation. A 1-cm-diameter hole was bore through the dome of the seal screw cap of the Falcon tube. A standard industrial Buna-N O-ring (113, 0.75-in. outer diameter) was inserted into the screw cap such that it rested below the threading. A 2-cm × 2-cm section of FTS H_2O flat sheet membrane was placed on the threaded end of the precut 15-mL tube with the feed side facing outward. The screw cap (with O-ring) was screwed into the 15-mL tube to secure the membrane with a leakproof seal. We note that the membrane was required to remain wet throughout assembly. Separately, two Pt flag electrodes (4 cm in length) were inserted through a red sleeve-type septum stopper (CG-3022–06, Chemglass Life Sciences) in a face-to-face orientation, with a 1-mL polypropylene divider positioned between them. A Ag/AgCl (3 M KCl, Leak-Free, Warner Instruments) reference electrode was inserted adjacent to the anode. The 15-mL Falcon tube with separator, electrodes, and electrolyte was outgassed during operation through a syringe needle to the atmosphere; for GC experiments, the necessary tubing was threaded through the septum in place of this needle. The gradation on the Falcon tube allowed for the internal volume to be roughly estimated throughout operation.

Electrochemical experiments were conducted on a CH Instruments 760D bipotentiostat. Cell potentials were converted to the SHE scale according to $E_{SHE} = E_{Ag/AgCl} + 0.197$ V. For faradaic efficiency measurements, the FOWS cell was operated under a constant flow of Ar gas (25 sccm) that was introduced through a gas inlet syringe. The gas outlet from the FOWS cell was connected to a GC equipped with a thermal conductivity detector (multiple gas analyzer 3, SRI Instruments). The amount of H_2 and O_2 in the out-fluxing Ar gas was quantified based on a calibration curve constricted from known H_2 and O_2 concentrations.

Phosphate Quantification. A Malachite green phosphate assay kit was used to determine P_i quantities in the outer electrolyte. The reaction of Malachite green with molybdate, and in the presence of P_i produces a green complex with an absorption maximum of 620 nm. Over a 48-h period of operation, three 250 μL aliquots of the outer electrolyte were taken at time points of 0, 24, and at 48 h. To 50 μL of these aliquots, 10 mL type I H_2O (200× dilution) was added and 800 μL of this resulting solution was combined with 200 μL of the Malachite green phosphate assay reagents (i.e., Malachite green and molybdate). The ultraviolet (UV)-vis absorption spectrum of these resulting solutions was then recorded using a Varian Cary 5000 spectrometer. The absorption at 650 nm was then compared to a seven-point standard curve (*SI Appendix*, Fig. S2), allowing the overall P_i concentration in the outer electrolyte to be quantified.

Chloride Quantification. A Lucigenin (10,10′-dimethyl-9,9′-biacridinium, dinitrate) fluorescent assay was used to determine the concentration of chloride in the inner electrolyte. The quenching of Lucigenin fluorescence by chloride was monitored at 505 nm. Over a 48-h period of operation, three 250 μL aliquots of the outer electrolyte were taken at time points of 0, 24, and at 48 h. To 62.5 μL of these aliquots, 1 mL type I H_2O (16× dilution) was added. To this resulting solution, 10 μL of a 1 mM Lucinegin solution in type I H_2O was added and the emission spectrum was recorded between 465 and 600 nm (λ_{exc} = 455 nm) using a PTI Technologies QuantaMaster 300 Fluorimeter. The emission at 505 nm was compared to a seven-point standard curve (*SI Appendix*, Fig. S3), allowing the overall Cl^- concentration in the inner electrolyte to be quantified.

Total HClO/ClO^- Quantification. A DPD assay was used to determine quantities of chloride oxidation products in the inner electrolyte. The DPD•$^+$-generated radical cation is red with an absorbance maximum of 531 nm. Over a 48-h period of operation, three 250 μL aliquots of the outer electrolyte were taken at time points of 0, 24, and at 48 h. To 62.5 μL of these aliquots, 1 mL type I H_2O (16× dilution) was added. To this resulting solution, 50 μL of a 500 mM DPD type I H_2O solution were added and the UV-vis absorption spectrum of these resulting solutions was recorded using a Varian Cary 5000 spectrometer. The absorption at 531 nm was compared to a seven-point standard curve of HClO/ClO^- concentrations (*SI Appendix*, Fig. S4), allowing the overall HClO/ClO^- concentration in the inner electrolyte to be quantified.

Data Availability. All study data are included in the article and/or *SI Appendix*.

Table 1. Quantification of key metrics for assessing FOWS cell performance

Hours	OER FE, %	HER FE, %	$[PO_4^{3-}]$, M	$[Cl^-]$, mM	$[ClO^-]$, mM	H_2O consumed, mL*	Stored energy, kJ†
0	100	100	0.800	6.15	0.03	0	0
24	100	100	0.790	41.2	0.11	2.02	27.12
48	100	100	0.776	33.8	0.28	4.04	54.24

*Calculated based on current passed and the observed 100% faradaic efficiency (FE) for water splitting.
†Based on quantity of H_2 generated.

ACKNOWLEDGMENTS. This work was performed under a Multidisciplinary University Research Initiative, sponsored by the Department of the Navy, Office of Naval Research, under Grant N00014-20-1-2418. We thank Matthew J. Nava, Bryan J. Kudisch, and Thomas P. Keane for helpful discussions. S.S.V. acknowledges support from the Herchel Smith Graduate Fellowship in the Sciences.

1. N. S. Lewis, D. G. Nocera, Powering the planet: Chemical challenges in solar energy utilization. *Proc. Natl. Acad. Sci. U.S.A.* **103**, 15729–15735 (2006).
2. A. Castillo, D. F. Gayme, Grid-scale energy storage applications in renewable energy integration: A survey. *Energy Convers. Manage.* **87**, 885–894 (2014).
3. B. Muruganantham, R. Gnanadass, N. P. Padhy, Challenges with renewable energy sources and storage in practical distribution systems. *Renew. Sustain. Energy Rev.* **73**, 125–134 (2017).
4. T. R. Cook *et al*., Solar energy supply and storage for the legacy and nonlegacy worlds. *Chem. Rev.* **110**, 6474–6502 (2010).
5. D. Gust, T. A. Moore, A. L. Moore, Solar fuels via artificial photosynthesis. *Acc. Chem. Res.* **42**, 1890–1898 (2009).
6. T. A. Faunce *et al*., Energy and environment policy case for a global project on artificial photosynthesis. *Energy Environ. Sci.* **6**, 695–698 (2013).
7. D. G. Nocera, Solar fuels and solar chemicals industry. *Acc. Chem. Res.* **50**, 616–619 (2017).
8. D. G. Nocera, The artificial leaf. *Acc. Chem. Res.* **45**, 767–776 (2012).
9. N. S. Lewis, D. G. Nocera, The solar opportunity. *Bridge* **45**, 41–47 (2015).
10. M. T. Spitler *et al*., Practical challenges in the development of photoelectrochemical solar fuels production. *Sustain. Energy Fuels* **4**, 985–995 (2020).
11. I. Shiklomanov, *Water in Crisis: A Guide to the World's Freshwater Resources* (Oxford University Press, 1993), chap. 2.
12. W. Tong *et al*., Electrolysis of low-grade and saline surface water. *Nat. Energy* **5**, 367–377 (2020).
13. S. Dresp, F. Dionigi, M. Klingenhof, P. Strasser, Direct electrolytic splitting of seawater: Opportunities and challenges. *ACS Energy Lett.* **4**, 933–942 (2019).
14. R. Balaji *et al*., An alternative approach to selective sea water oxidation for hydrogen production. *Electrochem. Commun.* **11**, 1700–1702 (2009).
15. L. Shi *et al*., Using reverse osmosis membranes to control ion transport during water electrolysis. *Energy Environ. Sci.* **13**, 3138–3148 (2020).
16. C. Costentin, D. G. Nocera, Self-healing catalysis in water. *Proc. Natl. Acad. Sci. U.S.A.* **114**, 13380–13384 (2017).
17. D. K. Bediako, A. M. Ullman, D. G. Nocera, Catalytic oxygen evolution by cobalt oxido thin films. *Top. Curr. Chem. (Cham)* **371**, 173–213 (2016).
18. A. S. Esswein, Y. Surendranath, S. Y. Reece, D. G. Nocera, Highly active cobalt phosphate and borate based oxygen evolving anodes operating in neutral and natural waters. *Energy Environ. Sci.* **4**, 499–504 (2011).
19. F. Dionigi, T. Reier, Z. Pawolek, M. Gliech, P. Strasser, Design criteria, operating conditions, and nickel-iron hydroxide catalyst materials for selective seawater electrolysis. *ChemSusChem* **9**, 962–972 (2016).
20. J. G. Vos, T. A. Wezendonk, A. W. Jeremiasse, M. T. M. Koper, MnOx/IrOx as selective oxygen evolution electrocatalyst in acidic chloride solution. *J. Am. Chem. Soc.* **140**, 10270–10281 (2018).
21. T. P. Keane, D. G. Nocera, Selective production of oxygen from seawater by oxidic metallate catalysts. *ACS Omega* **4**, 12860–12864 (2019).
22. M. Qasim, M. Badrelzaman, N. N. Darwish, N. A. Darwish, N. Hilal, Reverse osmosis desalination: A state-of-the-art review. *Desalination* **459**, 59–104 (2019).
23. D. S. Likhachev, F. C. Li, Large-scale water desalination methods: A review and new perspectives. *Desalination Water Treat.* **51**, 2836–2849 (2013).
24. T. K. Sherwood, P. L. T. Brian, R. E. Fisher, Desalination by reverse osmosis. *Ind. Eng. Chem. Fundam.* **6**, 2–12 (1967).
25. D. Li, H. Wang, Recent developments in reverse osmosis desalination membranes. *J. Mater. Chem.* **20**, 4551–4566 (2019).
26. H. K. Lonsdale, U. Merten, R. L. Riley, Transport properties of cellulose acetate osmotic membranes. *J. Appl. Polym. Sci.* **9**, 1341–1362 (1967).
27. B. S. Lalia, V. Kochkodan, R. Hashaikeh, N. Hilal, A review on membrane fabrication: Structure, properties and performance relationship. *Desalination* **326**, 77–95 (2013).
28. S. G. Carter, D. W. Karl, Inorganic phosphate assay with malachite green: An improvement and evaluation. *J. Biochem. Biophys. Methods* **7**, 7–13 (1982).
29. B. A. McNally, A. V. Koulov, B. D. Smith, J. B. Joos, A. P. Davis, A fluorescent assay for chloride transport; identification of a synthetic anionophore with improved activity. *Chem. Commun. (Camb.)* **8**, 1087–1089 (2005).
30. M. Pourbaix, *Atlas of Electrochemical Equilibria in Aqueous Solution* (NACE, 1974), p. 307.
31. D. L. Harp, *Current Technology of Chlorine Analysis for Water and Wastewater (Technical Information Series, Booklet No.17,*Hach Company, 2002).
32. T. O'Brien, T. Bommaraju, F. Hine, "Chemistry and electrochemistry of the chlor-alkali process" in *Handbook of Chlor-Alkali Technology* (Springer, 2005), vol. I, pp. 75–386.